A data fusion approach for combined Terrestrial Radar Interferometry (TRI) and Robotic Total Station (RTS) monitoring

Nicola DAL SANTO[1,*] and **Alberto MICHELINI**[1]

[1] *IDS GeoRadar, Pisa, Italy, (nicola.dalsanto@idsgeoradar.com)*

[*] *corresponding author*

Abstract

Terrestrial Radar Interferometry (TRI) and Robotic Total Station (RTS) are nowadays two well-established monitoring techniques used in numerous fields of application, including open-pit mining, civil engineering, natural hazard prevention. These two technologies have rather complementary characteristics, in fact RTS provides a measurement of the 3D displacement on specific points while TRI provides a dense 1D map of the Line of Sight (LoS) displacement component. More and more frequently, TRI and RTS are often used simultaneously within the same monitoring campaign, to improve the redundancy of the overall monitoring system. Furthermore, their complementarity makes them excellent candidates to be combined to improve the information gathered from monitoring data. This work aims to present a data fusion approach that allows the estimation of a dense deformation vector field starting from RTS and TRI measurements. The proposed methodology has been applied on a slope monitoring dataset, in order to verify its validity and evaluate possible limitations.

Keywords: Terrestrial Radar Interferometry, Robotic Total Stations, prisms, data fusion, vector field

Received: 9^{th} December 2024. Revised: 14^{th} March 2025. Accepted: 14^{th} March 2025.

1 Introduction

Slope deformation monitoring is a critical activity, which has become even more important over the years due to climate change and the ever-increasing number of man-made slopes, such as those present in open-pit mines (Sharon, 2020). Currently, among the numerous methods available to carry out this type of monitoring, probably the two most successful are Robotic Total Stations (RTS) and Terrestrial Radar Interferometry (TRI).

RTS are optical surveying instruments that can measure distance and horizontal/vertical angles of specific targets (prisms), from which the corresponding three-dimensional Cartesian coordinates can be obtained by triangulations. RTS integrates automatic positioning and automatic target recognition, enabling faster and more accurate measurements with no need for human supervision. These features make RTS particularly suitable for continuous monitoring (Afeni and Cawood, 2013), where accurate knowledge of three-dimensional deformation is required.

TRI is a class of remote sensing techniques based on coherent radar systems (Caduff et al., 2015), whose operating principle is to transmit signals in the microwave frequency band and collect the backscattered echoes coming from the objects present inside the radar Field of View (FoV). Through radar imaging techniques, TRI systems are able to reconstruct a complex-valued image of the scenario, where for each pixel the amplitude and the phase of the microwave signal are measured. Exploiting interferometric techniques, from phase variations it is possible to extract the Line of Sight (LoS) displacement of targets contained within the radar pixel, with submillimeter precision. The final product of the TRI measurement is a streaming of LoS displacement maps that is automatically updated at every new acquisition. Thanks to its unique features, TRI has become the state of the art for open-pit mine slope monitoring (Bar et al., 2022). The use of this technology is not limited to the mining sector (Pieraccini and Miccinesi, 2019), but finds numerous applications in the monitoring of natural geohazards, such as landslides, glaciers, and volcanoes, as well as in

the monitoring of complex structures such as buildings, bridges, and dams (Rebmeister, 2024).
In a nutshell, RTS provides the three-dimensional displacement at specific measurement points, while TRI provides the one-dimensional LoS displacement over a distributed map of the scenario. Given the complementary nature of their deformation measurements, RTS and TRI are increasingly used in combination to improve the redundancy of the overall monitoring system (Rodriguez et al., 2024). Furthermore, their complementarity makes them excellent candidates to be combined to improve the information gathered from monitoring data. This work aims to present a data fusion approach that allows the estimation of a dense deformation vector field starting from RTS and TRI measurements. Section 2 provides a background on the data acquired by the RTS and TRI systems and outlines the problem that is intended to be addressed. Section 3 describes the proposed method for estimating the deformation vector field starting from monitoring data. Finally, in section 4 the proposed method is applied on a real case study. Before presenting the developed method, it is worthwhile to remember that over the years various approaches have been proposed to obtain a continuous deformation vector field from the combination of different terrestrial monitoring systems. Among the methods that are based on TRI, it is possible to mention the integration with optical Digital Image Correlation (DIC) (Elmouttie et al., 2021) (Dematteis et al., 2018) as well as the integration with Terrestrial Laser Scanner (TLS) (Tapete et al., 2013). While among those based on the use of RTS, there are methods that exploit pure interpolation (Manconi et al., 2013) or integration with DIC (Dematteis et al., 2022). Compared to these works, the present choice of combining TRI and RTS is justified not only by the strong systems complementarity, but also by their widespread diffusion in mining applications. An effective data fusion method would therefore be immediately applicable to most existing slope monitoring campaigns.

2 Background

The object of slope monitoring is the surface deformation of natural or man-made slopes, whose understanding of 3D behavior is essential to determine its stability condition and therefore the associated risk factors (McQuillan and Bar, 2023). The surfaces of monitored slopes can be represented by a set of 3D points (point cloud) or a set of polygonal faces (polygon mesh). The generic surface representation will be denoted by $\mathscr{S}$. Given two collected epochs, the most complete information on surface deformation is given by the three-dimensional deformation vector field $\mathbf{u}(\mathbf{x})\ \mathbf{x} \in \mathscr{S}\ \mathbf{u} \in \mathbb{R}^3$.
Generally, only a partial measurement of this vector field can be made with a single monitoring method.

2.1 RTS Data

RTS monitoring provides the measurement of 3D position at some predefined points $\mathbf{x}_n$, $n = 1,\dots,N$, where prisms have been installed. Comparing two epochs, it is possible to extract the 3D deformation vector $\mathbf{u}_n$ for each measurement point (figure 1).
If the RTS measures are not affected by bias, their expectation values are equal to the deformation vector evaluated at those points:

$$\mathrm{E}[\mathbf{u}_n] = \mathbf{u}(\mathbf{x}_n) \tag{1}$$

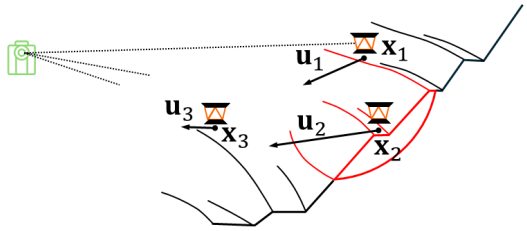

Figure 1. RTS measurement, three prisms located in $\mathbf{x}_1$, $\mathbf{x}_2$ and $\mathbf{x}_3$, are measured by a RTS obtaining three corresponding displacement vectors $\mathbf{u}_1$, $\mathbf{u}_2$ and $\mathbf{u}_3$

In a well-performed monitoring campaign, together with the displacement measurements, the corresponding covariance matrices $\mathbf{\Sigma}_{nm}$ should also be available:

$$\mathbf{\Sigma}_{nm} = \mathrm{E}[\mathbf{u}_n\mathbf{u}_m^{\mathrm{T}}] - \mathrm{E}[\mathbf{u}_n]\mathrm{E}[\mathbf{u}_m^{\mathrm{T}}] \tag{2}$$

Where $n,m = 1,\dots,N$ are the prisms indices. For sake of simplicity, in the following the availability of these matrices will not be required, and homoscedasticity will be assumed. Nevertheless, the

introduction of RTS measurements covariance inside the equations, would allow a greater robustness and accuracy of the results.

2.2 TRI Data

TRI systems exploit radar imaging techniques to acquire complex-valued images of the monitored scenario. Applying interferometric methods to those images, it is possible to measure the deformation vector component along radar LoS direction $\mathbf{e}(\mathbf{x})$ for each image's pixel (Monserrat et al., 2014). LoS deformation measure is usually denoted with $\Delta r(\mathbf{x})$ being the range variation between the radar sensor and the measured point (figure 2).

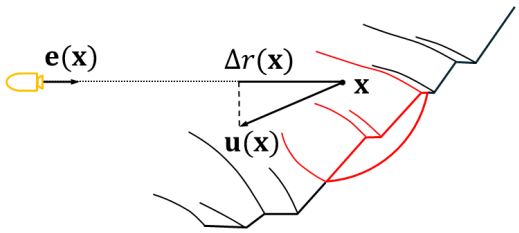

Figure 2. TRI measurement, the range variation is the projection of deformation vector along the radar LoS

To obtain the final TRI measurement, a complicated data processing is necessary to remove the atmospheric contributions to the interferometric phase (Michelini et al., 2014). Given the complexity of this procedure, it is not always justified to assume that TRI measurements are free from bias, as they may contain some atmospheric residuals, not perfectly compensated by the processing. In this work, we will therefore assume that the TRI measurements are affected by a bias $b(\mathbf{x})$:

$$\mathrm{E}[\Delta r(\mathbf{x})] = \mathbf{u}(\mathbf{x}) \cdot \mathbf{e}(\mathbf{x}) + b(\mathbf{x}). \tag{3}$$

It is however legitimate to assume that this atmospheric bias is a spatially smooth function, expandable into a limited number of analytic functions, which are better suited to model the spatial distribution of the atmosphere:

$$b(\mathbf{x}) = \sum_{k=1}^{K} b_k f_k(\mathbf{x}). \tag{4}$$

Without additional data other than radar ones, it is in general not possible to deduce any information about the unknown coefficients b_k. However, by having external data sources, such as RTS measurements, it is possible to estimate the coefficients b_k and thus remove the bias from the radar measurements.
Also for radar data, in principle, the measurements covariance $\sigma^2(\mathbf{x},\mathbf{y})$ could be available, but again it will not be required in the proposed method.

2.3 Problem formulation

Having defined the information provided by RTS and TRI, it is now possible to outline the goal of the data fusion method presented in this paper. The problem that is intended to be addressed can be described as follows: given N 3D deformation measurement $\mathbf{u}_n$ localized in $\mathbf{x}_n$ and a dense 1D measurement $\Delta r(\mathbf{x})$ of the deformation component along LoS directions $\mathbf{e}(\mathbf{x})$, what is the best estimation $\hat{\mathbf{u}}(\mathbf{x})$ of the underlying deformation vector field $\mathbf{u}(\mathbf{x})$? Since this is fundamentally an interpolation problem (Chiles and Delfiner, 2012), there is not an unique answer, but the specific solution depends strongly on the characteristics of the underlying phenomenon that is trying to be modelled. In this case the object of interpolation is the slope surface deformation, and with this in mind, it is possible to discuss some simple hypotheses on it.

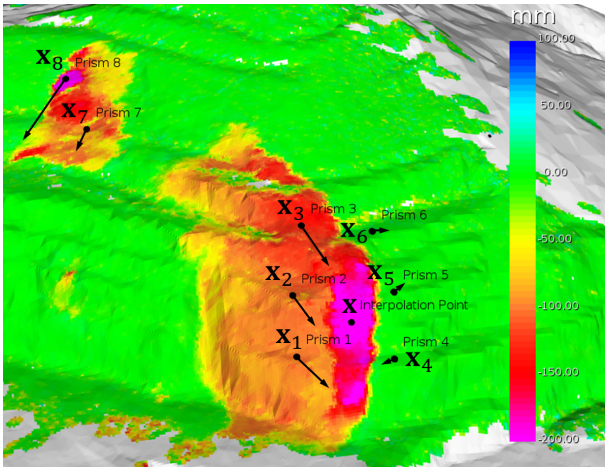

Figure 3. Example of RTS and TRI slope deformation measurement

To better present the assumptions that are made about the generic deformation vector field of a

slope, let's consider the specific example of RTS and TRI measurement represented in figure 3. In this case, eight RTS measurement points are placed inside a TRI LoS deformation map.
If one seeks what can be the most accurate estimate of the deformation vector at the point $\mathbf{x}$, denoted as the interpolation point, it is clear that for the calculation it should be considered only prisms 1, 2 and 3, since they belong to the same movement process. While, despite being spatially close to $\mathbf{x}$, prisms 4, 5 and 6 should not be taken into account, since they belong to a motionless zone, and therefore the vector measured by them will likely be dominated by noise. On the other hand, prisms 7 and 8, even if they show a LoS displacement comparable to the point considered, must not be used in the estimation of the deformation vector, since they belong to a spatially disconnected moving area. Thus, the first observation is that a correlation measure of the displacement based on geometric and/or geostatistical criteria is necessary.
At this point, having selected only prisms 1, 2 and 3, it is possible to notice that the LoS deformation in the interpolation point is greater than any LoS deformation measured by any of the three prisms. This can be explained by two opposite assumptions: it is possible to consider the deformation vector direction to be roughly similar to the prisms one, while its magnitude increases at the interpolation point:

$$\hat{\mathbf{u}}(\mathbf{x}) \sim \frac{\Delta r(\mathbf{x})}{\mathbf{u}_n \cdot \mathbf{e}(\mathbf{x})} \mathbf{u}_n. \tag{5}$$

Conversely, it is possible to assume that the vector magnitude remains constant while its direction becomes more aligned with the radar LoS:

$$\hat{\mathbf{u}}(\mathbf{x}) \sim \mathbf{u}_n + (\Delta r(\mathbf{x}) - \mathbf{u}_n \cdot \mathbf{e}(\mathbf{x}))\mathbf{e}(\mathbf{x}) \tag{6}$$

Since the TRI location is arbitrary and independent from the actual slope displacement, requiring an alignment along its LoS direction (6) seems an unrealistic imposition. For this reason, in the proposed method, the vector rescaling hypothesis (5) will be preferred to the vector alignment one.
This specific example is meant to illustrate the more generic slope monitoring cases, where various deformation processes coexist, and even within a single process, the vector field can be quite variable. Clearly, the most generic slope monitoring case may present even more complex aspects (e.g., deformation processes with overlaps or complex discontinuities) whose management goes beyond the scope of this work.

3 Method

Having defined the main characteristics of the data acquired by RTS and TRI, together with the assumptions made for the interpolation, it is now possible to describe the details of the proposed method.

3.1 TRI calibration

The first step of the method consists of the removal of TRI measurement bias due to the atmospheric residuals. The TRI measurement calibration is performed by exploiting the RTS measurements. To this purpose, combining expectation values equations (1) and (3), it is possible to derive a relation for TRI bias evaluated in RTS measurement points:

$$b(\mathbf{x}_n) = \mathrm{E}[\Delta r(\mathbf{x}_n)] - \mathrm{E}[\mathbf{u}_n \cdot \mathbf{e}(\mathbf{x}_n)], \tag{7}$$

which simply tells us that it is possible to provide a bias coefficients estimation $\hat{b}_k$, by comparing the TRI measurements with the RTS measurements projected along the radar LoS direction. The coefficients can be estimated by means of a least square regression that minimizes the following functional:

$$\sum_{n=1}^{N} [b(\mathbf{x}_n) + \mathbf{u}_n \cdot \mathbf{e}(\mathbf{x}_n) - \Delta r(\mathbf{x}_n)]^2 \tag{8}$$

and then used to remove the measurement bias from TRI data

$$\Delta r(\mathbf{x}) \to \Delta r(\mathbf{x}) - \sum_{k=1}^{K} \hat{b}_k f_k(\mathbf{x}) \tag{9}$$

In figure 4 is shown a TRI map with the correspondent RTS LoS measurements. the comparison between a radar map before and after a calibration. It is possible to notice that, at a qualitatively level, there is a good correspondence between the two datasets but, quantitatively, the RTS tends to measure a higher LoS deformation than the TRI.

After the calibration procedure (figure 5), the two datasets also agree on a quantitative level. However, it should be noted that outside the prism network, at the right and lower-left boundaries of the map, the calibration procedure introduced unrealistic results. These are typical effects due to extrapolation, and for this reason, only results that fall within the prism network should be considered.

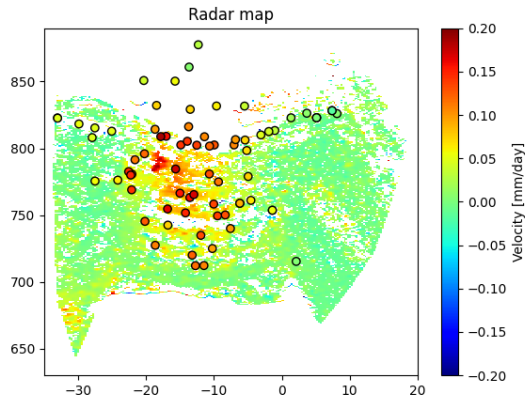

Figure 4. Uncalibrated radar map, overlaid with prism measurements projected onto the TRI LoS

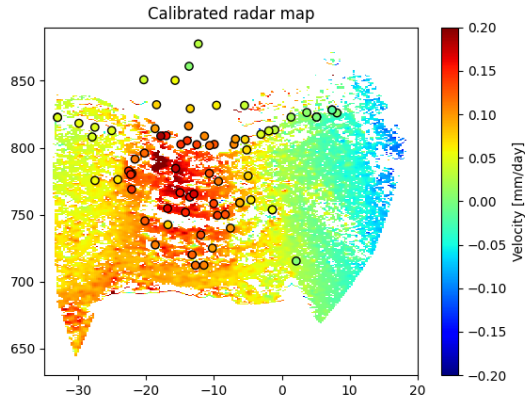

Figure 5. Calibrated radar map, overlaid with prism measurements projected onto the TRI LoS

3.2 Vector field estimation

Once the potential bias has been removed from the TRI measurements, and thus having ensured that the two datasets are consistent with each other, it is possible to proceed with the computation of vector field estimation $\hat{\mathbf{u}}(\mathbf{x})$. As mentioned in section 2.3, this can be considered as an interpolation problem; therefore, the estimated vector field can be decomposed as:

$$\hat{\mathbf{u}}(\mathbf{x}) = \sum_{n=1}^{N} \lambda_n(\mathbf{x})\mathbf{u}_n \tag{10}$$

where $\lambda_n(\mathbf{x})$ are unknown coefficients to be determined. In standard interpolation problems, this relation is complemented by a normalization constraint on the coefficients. However, in this case, normalization to one is not compatible with the constraint given by the TRI measures, which can be written as follows:

$$\sum_{n=1}^{N} (\mathbf{u}_n \cdot \mathbf{e}(\mathbf{x}))\lambda_n(\mathbf{x}) = \hat{\mathbf{u}}(\mathbf{x}) \cdot \mathbf{e}(\mathbf{x}) = \Delta r(\mathbf{x}) \tag{11}$$

Therefore, to follow the TRI observations, instead of the usual normalization, the constraint (11) will be imposed on the interpolation coefficients. For the sake of simplicity, let's now suppose to know a correlation measure $\rho(\mathbf{x}, \mathbf{x}_n)$ of slope deformation between the point $\mathbf{x}$ and points $\mathbf{x}_n$. This correlation function should incorporate the criteria discussed in section 2.3, and it could be calculated on the basis of geometric, statistical, or geological concepts (Li and Heap, 2023) (Chiles and Delfiner, 2012). In the present work, a purely geometric measure was used, based on the distance between the points: $\rho(\mathbf{x}, \mathbf{x}_n) \propto |\mathbf{x} - \mathbf{x}_n|^{-2}$ nevertheless, for future developments, it would be desirable to be able to define a measure that exploits statistical information like variograms or geological information like discontinuity planes.
Measurements that come from prisms whose deformation is completely uncorrelated to the one under examination should not contribute to the corresponding interpolation. To enforce these requirements, it is plausible to assume that good interpolation coefficients $\lambda_n(\mathbf{x})$ should be proportional to the correlation function. To express this requirement, auxiliary coefficients $\kappa_n(\mathbf{x})$ are introduced:

$$\lambda_n(\mathbf{x}) = \kappa_n(\mathbf{x})\rho(\mathbf{x}, \mathbf{x}_n) \tag{12}$$

The last requirement, which allows the interpolation coefficients final calculation, is the minimization of $\hat{\mathbf{u}}(\mathbf{x})$ variance. This can be done by minimizing the following cost function F,

$$F = \frac{1}{2}(\mathrm{E}[\hat{\mathbf{u}}(\mathbf{x}) \cdot \hat{\mathbf{u}}(\mathbf{x})] - \mathrm{E}[\hat{\mathbf{u}}(\mathbf{x})] \cdot \mathrm{E}[\hat{\mathbf{u}}(\mathbf{x})]) - \mu(\mathrm{E}[\hat{\mathbf{u}}(\mathbf{x})] \cdot \mathbf{e}(\mathbf{x}) - \Delta r(\mathbf{x})) \tag{13}$$

where a Lagrange multiplier μ has been introduced to enforce the condition (11). Inserting equations 10 and 12 in this functional and exploiting the simple homoschedasticity assumption it is possible to rephrase the minimization problem in terms of coefficients κ_n:

$$F(\kappa_n, \mathbf{x}) = \frac{1}{2}\sum_{n=1}^{N} \rho^2(\mathbf{x}, \mathbf{x}_n)\kappa_n^2 - \mu(\sum_{n=1}^{N} \rho(\mathbf{x}, \mathbf{x}_n)(\mathbf{u}_m \cdot \mathbf{e}(\mathbf{x}))\kappa_n - \Delta r(\mathbf{x})) \tag{14}$$

The minimization of F leads to an expression for $\kappa_n(\mathbf{x})$ which, when inserted into the equations (12) and (10), allows to obtain the searched deformation vector estimation:

$$\hat{\mathbf{u}}(\mathbf{x}) = \frac{\Delta r(\mathbf{x}) \sum_{n=1}^{N} \rho(\mathbf{x}, \mathbf{x}_n)(\mathbf{u}_n \cdot \mathbf{e}(\mathbf{x}))\mathbf{u}_n}{\sum_{m=1}^{N} \rho(\mathbf{x}, \mathbf{x}_m)(\mathbf{u}_m \cdot \mathbf{e}(\mathbf{x}))^2} \tag{15}$$

As expected, this expression satisfies the TRI constraint (11), furthermore, it suppresses the contributions of prisms for which $\rho(\mathbf{x}, \mathbf{x}_n)$ or $\mathbf{u}_n \cdot \mathbf{e}(\mathbf{x})$ are almost zero.

4 Case study

To illustrate the potential of TRI and RTS data fusion, the proposed method was applied on a real open-pit monitoring campaign. The scenario considered is an open-pit gold mine, approximately 3.3 km wide and 550 m deep. RTS and TRI systems were installed in front of the pit's south-wall and acquired continuously for a month. RTS surveyed a total of 47 prisms deployed along the slope, whereas TRI was able to measure the LoS ground displacement of 250 thousand radar pixels distributed on the terrain surface. The slope had several zones of motion, with various spatial extensions and various rates and directions of deformation, and it is therefore a good test site to evaluate the potential of the proposed method.
In this example, the correlation measure $\rho(\mathbf{x}, \mathbf{x}_n)$ was calculated on the basis of pure geometric aspects as explained in the previous section. The final results of the entire data fusion algorithm are presented in figure 6 and figure 7, where the measured prisms vectors (in light blue) and the estimated vector field (in black) are overlaid on the calibrated TRI map.

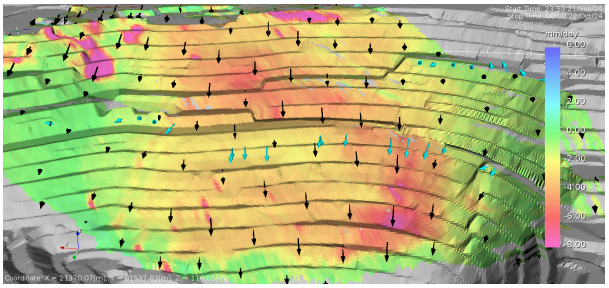

Figure 6. Case study, data fusion vector field global view

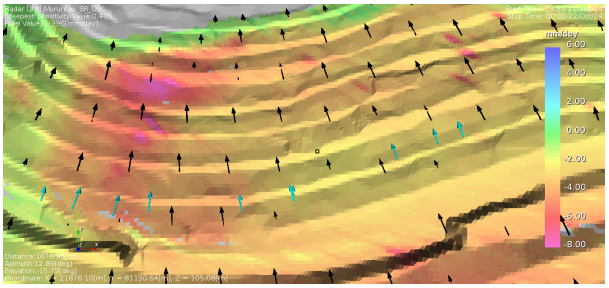

Figure 7. Case study, data fusion vector field detailed top view

From these figures, it can be seen that the orientation and magnitude of the vector field densely interpolate the three-dimensional slope behaviour, allowing for better interpretation of the kinematics of movements observed in the slope. In particular, in figure 7 is shown the top view of the resulting vector field, where it is possible to notice that the deformation vectors align well along the slope's steepest direction, as expected from a gravity-induced phenomenon.
However, it is important to remark that due to the sparse distribution of prisms, various moving areas covered by the TRI map are not adequately surveyed by the RTS. As an example, in figure 8 it is possible to observe a portion of the south-est wall where no prisms are installed, despite different kinds of deformations have been revealed by the TRI monitoring. In particular, it is possible to

observe a fast-moving area where no prism has been installed inside. In this specific area, the vector field is oriented obliquely respect to the steepest direction of the slope, and even in the absence of a ground truth, it is plausible to assume that the estimated vector does not correspond to the real deformation direction.

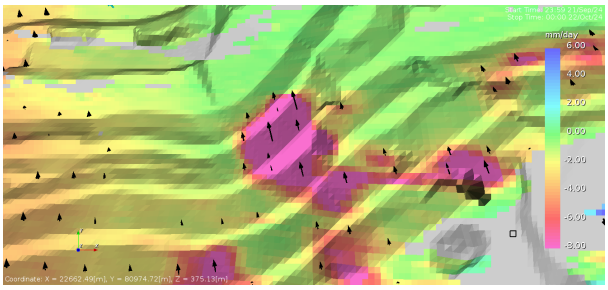

Figure 8. Case study, data fusion vector field south east wall

The misalignment occurs because, to reconstruct this vector, prisms measurements from uncorrelated deformation processes were used. This unwanted condition can be properly mitigated only if an adequate spatial sampling of prisms is available. In cases like the present one, where the prisms do not adequately sample all the deformation processes, it would be desirable to develop a method to determine at which points it makes sense to reconstruct the vector field and at which points it is not possible to provide a reliable estimation. In order to do that, it is probably necessary to introduce inside the correlation measure computation, some geostatistical factors that describe the degree of dependence of the various slope movements. With this information it should then be possible to determine whether a given interpolation point has enough prisms related to it for the vector reconstruction.

5 Conclusion

In this work, the fusion of RTS and TRI monitoring data has been investigated by proposing a method for the estimation of three-dimensional deformation vector field. From the analysis of section 2.3, it is clear that there is a strong potential for the integration of these two monitoring systems. TRI provides a density and continuity of measurements not obtainable with prisms survey. On the other hand, RTS data can help to calibrate RTS results. A method that allows the fusion of data acquired by RTS and TRI would bring an immediate benefit, especially in the open-pit mine monitoring sector, where both technologies are already used in combination. The method proposed in this work was tested on a typical mining scenario; the resulting vector field shown in section 4 clearly demonstrates the potential and usefulness of this approach in open-pit slope monitoring. The method still has some limitations, particularly related to the vector extrapolation in areas not adequately covered by the prisms. To address these limitations, in section 4 a possible strategy has been proposed. Starting from the concepts presented in this work, there are several future developments that could significantly enhance the method proposed here. Among them, it is worth mentioning the possibility of combining RTS data with those coming from multiple independent radar systems, whether they are terrestrial or satellite-based. This redundancy of measurements will surely lead to more accurate and reliable results.

References

Afeni, T. B. and Cawood, F. T. (2013). Slope monitoring using total station: what are the challenges and how should these be mitigated? *South African Journal of Geomatics*, 2(1):41–53.

Bar, N., Cobian, J., Bautista, M., Mojica, B., Coli, N., Preston, C., Ribeiro, R., Bueno, G., and Lopes, L. (2022). Brittle and ductile slope failure management. *Proceedings of Slope Stability*, pages 17–21.

Caduff, R., Schlunegger, F., Kos, A., and Wiesmann, A. (2015). A review of terrestrial radar interferometry for measuring surface change in the geosciences. *Earth surface processes and landforms*, 40(2):208–228.

Chiles, J. and Delfiner, P. (2012). *Geostatistics: modeling spatial uncertainty*. Wiley.

Dematteis, N., Giordan, D., Zucca, F., Luzi, G., and Allasia, P. (2018). 4d surface kinematics monitoring through terrestrial radar interferometry and image cross-correlation coupling. *ISPRS journal of photogrammetry and remote sensing*, 142:38–50.

Dematteis, N., Wrzesniak, A., Allasia, P., Bertolo, D., and Giordan, D. (2022). Integration of robotic

total station and digital image correlation to assess the three-dimensional surface kinematics of a landslide. *Engineering Geology*, 303:106655.

Elmouttie, M. K., Luo, X., Dean, P., Duan, J., and Malos, J. (2021). Slope monitoring using sensor fusion. *SSIM 2021: Second International Slope Stability in Mining*, pages 199–210.

Li, J. and Heap, A. (2023). A review of spatial interpolation methods for environmental scientists. *Technical Report 2008/023, Geoscience Australia*, pages 137–145.

Manconi, A., Allasia, P., Giordan, D., Baldo, M., Lollino, G., Corazza, A., and Albanese, V. (2013). Landslide 3d surface deformation model obtained via rts measurements. *Landslide Science and Practice: Volume 2: Early Warning, Instrumentation and Monitoring*, pages 431–436.

McQuillan, A. and Bar, N. (2023). The necessity of 3d analysisfor open-pit rock slope stability studies: theory and practice. *Journal of the SouthernAfrican Institute of Mining andMetallurgy*, 123(2):63–70.

Michelini, A., Coli, N., Coppi, F., Farina, P., Leoni, L., Sà, G., and Costa, T. (2014). Advanced data processing of ground-based synthetic aperture radar for slope monitoring in open pit mines. *Proceedings of the 2015 24th International Mining Congress of Turkey*, pages 420–427.

Monserrat, O., Crosetto, M., and Luzi, G. (2014). A review of ground-based sar interferometry for deformation measurement. *ISPRS Journal of Photogrammetry and Remote Sensing*, 93:40–48.

Pieraccini, M. and Miccinesi, L. (2019). Ground-based radar interferometry: A bibliographic review. *Remote Sensing*, 11(9):1029.

Rebmeister, M. (2024). *Geodetic monitoring of complex shaped infrastructures using Ground-Based InSAR*. PhD thesis, Karlsruhe Institute of Technology.

Rodriguez, S., Bianchetti, F., Giliberto, F., Michelini, A., Benedetti, A., Fernandez, D., Fernandez, J., Diaz, M., Tarife, A., Sanchez, P., and S., D. (2024). Atalaya tsf monitoring: Data correlation, modelling and best practices. *New Challenges in Rock Mechanics and Rock Engineering*, pages 921–926.

Sharon, R. (2020). Slope performance monitoring: system design, implementation and quality assurance. *Proceedings of the 2020 International Symposium on Slope Stability in Open Pit Mining and Civil Engineering*, pages 17–38.

Tapete, D., Casagli, N., Luzi, G., Fanti, R., Gigli, G., and Leva, D. (2013). Integrating radar and laser-based remote sensing techniques for monitoring structural deformation of archaeological monuments. *Journal of Archaeological Science*, 40(1):176–189.